

Poisson type conformastat spherically symmetric anisotropic fluid spacetimes

Gonzalo García-Reyes*

Departamento de Física, Universidad Tecnológica de Pereira, A. A. 97, Pereira, Colombia

We construct conformastat spherically symmetric spacetimes representing anisotropic fluid matter distributions from given solutions of the Poisson's equation of Newtonian gravity and its corresponding circular speed profile. As simple examples, we present three families of spherically symmetric spacetimes which we apply in constructing new models of relativistic anisotropic thick spherical shells, and of relativistic galaxy models composite by a central spherical bulge, the thick disk and the dark matter halo, writing in this case the metric in cylindrical coordinates. Moreover, the geodesic motion of test particles in stable circular orbits around such structures is studied. We build anisotropic fluid sources for these spacetimes which satisfy all the energy conditions and the principal stresses are positive quantities (pressure).

I. INTRODUCTION

Spherically symmetric distributions of matter are important in relativistic astrophysics as models of neutron stars, highly dense stars, gravastars, dark energy stars, quark stars and galactic nuclei. Spherical shells are also useful in astrophysics as models of supernovas, in general relativity to analyze basic issues of gravitational collapse and as sources of vacuum gravitational fields, and in cosmology [1]. Anisotropic thick spherical shell models as sources of static spherically symmetric spacetimes built from Newtonian potential-density pairs in isotropic coordinates were studied in Refs. [2, 3] for a Schwarzschild type metric and in Ref. [4] for Majumdar-Papapetrou type fields. This same approach has also been used in building perfect fluid sources for these spacetimes [5] and regarding static axisymmetric fields in the investigation of anisotropic galaxy relativistic models for a Schwarzschild type metric [6] and in Ref. [7] in constructing three-dimensional sources for Majumdar-Papapetrou type fields.

In this work, we build conformastat spherically symmetric spacetimes which we apply in constructing new relativistic models of anisotropic thick spherical shells and galaxies from Newtonian potential-density pairs and its corresponding circular speed profile. As in the references cited above, one of the metric functions, the spatial components of the metric, is obtained of the fact that one of the field equations is a nonlinear Poisson type equation. This equation is solved for a particular energy density profile which is chosen by demanding that in Newtonian limit it reduces to its Newtonian value. The other metric function, the temporal component of the metric, is obtained analytically in this work by kinematic considerations by also requiring that in the Newtonian limit the relativistic circular speed profile reduces to its Newtonian value.

The paper is structured as follows. In Section II, in order to calculate the spatial components of the metric, we summarize the method to build different compact sources for conformastat spherically symmetric spacetimes from given solutions of Poisson's equation. On the other hand, to compute the temporal component of the metric, we also analysis the geodesic circular motion of test particles moving on a static spherically symmetric spacetime in isotropic coordinates and the stability of the orbits against radial perturbations. In Section III, for a given specific circular speed profile, three families of spherically symmetric anisotropic fluid spacetimes are obtained, and, as a simple application, new models of relativistic thick spherical shells are constructed for some members of the families.

In Section IV, such metrics are also used in building two three-component relativistic models of galaxies (bulge, disk and dark matter halo) using as seed Newtonian potential-density pairs the Miyamoto-Nagai potentials for the central bulge and the disk [8, 9] and for the dark matter halo the well-known Navarro-Frenk-White (NFW) model [10]. Since the disk-like component are structures with axial symmetry, in this case the metric is written in cylindrical coordinates. Such spacetimes can be interesting not only from the merely theoretical point of view but also, for example, in describing galactic nuclei where relativistic effects are expected to be important. Finally, in Section V we summarize the results obtained.

* e-mail: ggarcia@utp.edu.co

II. POISSON TYPE SPACETIMES AND MOTION OF PARTICLES

The metric for a conformastat spherically symmetric spacetime is given by [11, 12]

$$ds^2 = -e^{2\nu(r)}dt^2 + e^{2\lambda(r)}(dr^2 + r^2d\Omega^2), \quad (1)$$

where $d\Omega^2 = d\theta^2 + \sin^2\theta d\varphi^2$. The term “conformastat” means that spatial metric is conformally flat. The units are chosen so that we have for the speed of light in vacuum $c = 1$. Einstein’s gravitational field equations $G_{ab} = 8\pi GT_{ab}$ yield the following non-zero components of the energy-momentum tensor

$$T^t_t = \frac{1}{4\pi G}e^{-2\lambda} \left[\nabla^2\lambda + \frac{1}{2}\nabla\lambda \cdot \nabla\lambda \right], \quad (2a)$$

$$T^r_r = \frac{1}{8\pi G}e^{-2\lambda} \left[(\lambda')^2 + 2\lambda'\nu' + \frac{2}{r}(\lambda' + \nu') \right], \quad (2b)$$

$$T^\theta_\theta = T^\varphi_\varphi = \frac{1}{8\pi G}e^{-2\lambda} \left[\lambda'' + \nu'' + (\nu')^2 + \frac{1}{r}(\lambda' + \nu') \right], \quad (2c)$$

where primes indicate differentiation with respect to r . The expression (2a) for the T^t_t component of the energy-momentum tensor holds even if spatial symmetry is not assumed for the gravitational field, in other words, in the case that metric functions be a function of all spatial coordinates.

With respect to the orthonormal tetrad or locally Minkowskian observer

$$\mathbf{V} = \frac{1}{\sqrt{-g_{tt}}}(1, 0, 0, 0), \quad (3a)$$

$$\mathbf{X} = \frac{1}{\sqrt{g_{rr}}}(0, 1, 0, 0), \quad (3b)$$

$$\mathbf{Y} = \frac{1}{\sqrt{g_{\theta\theta}}}(0, 0, 1, 0), \quad (3c)$$

$$\mathbf{Z} = \frac{1}{\sqrt{g_{\varphi\varphi}}}(0, 0, 0, 1), \quad (3d)$$

whose components are denoted as $e_{(a)}^b = \{V^b, X^b, Y^b, Z^b\}$, where Latin indices a and b run from 0 to 3, the relativistic energy density is given by $\rho = -T^t_t$, and the principal stresses (pressures or tensions) by $p_i = T^i_i$.

By setting

$$e^{2\lambda} = \left(1 - \frac{\phi(r)}{2}\right)^4, \quad (4)$$

we get, even without spatial symmetry, for the energy density the following nonlinear Poisson type equation

$$\nabla^2\phi = 4\pi G\rho \left(1 - \frac{\phi}{2}\right)^5, \quad (5)$$

In fact, in Newtonian limit when $\phi \ll 1$ it reduces to Poisson’s equation, $\nabla^2\Phi = 4\pi G\rho_N$. For a given physical energy density profile ρ , the metric function ϕ can be obtained by resolving this equation. A physically reasonable way to choose ρ is by requiring that in the Newtonian limit it reduces to its Newtonian value ρ_N . A simple particular form of ρ which satisfies such condition is

$$\rho = \frac{\rho_0}{\left(1 - \frac{\phi}{2}\right)^5}. \quad (6)$$

Replacing this expression in (5) one finds in this case that the pair (ϕ, ρ_0) is a solution of the Poisson’s equation. In conclusion, for each Newtonian solution there is a relativistic one such that $(\Phi, \rho_N) \rightarrow (\Phi, \rho_N/(1 - \Phi/2)^5)$, where the first pair solves the Poisson equation while the latter one solves (5).

Accordingly, such geometries can be called Poisson type spacetimes. For example, the pair $(\phi, \rho_0) = (-\frac{MG}{r}, 0)$ corresponds to the external Schwarzschild solution in isotropic coordinates. To obtain the other metric function ν an additional assumption must be imposed and will be obtained in next section by kinematic considerations.

A. Stable circular orbits

With respect to the comoving frame of reference (3a) - (3d), the 4-velocity \mathbf{u} of a test particle moving on the spacetime (1) has components

$$u^{(a)} = e^{(a)}{}_b u^b, \quad (7)$$

and the 3-velocity \mathbf{v}

$$v^{(i)} = \frac{u^{(i)}}{u^{(t)}} = \frac{e^{(i)}{}_a u^a}{e^{(t)}{}_b u^b}. \quad (8)$$

Because of its mathematical simplicity and astrophysical relevance, we shall consider circular orbits. For instance, the stars of the disk in spiral galaxies travel in nearly circular orbits around the galactic center [13]. In addition, due to the spherical symmetry and also for simplicity, we shall analyze equatorial orbits on the plane $\theta = \pi/2$. Thus, for equatorial, circular orbits $dr/dt = d\theta/dt = 0$, then $\mathbf{u} = u^t(1, 0, 0, \omega)$, where $\omega = u^\varphi/u^t = d\varphi/dt$ is the angular speed of the test particles. In this case $v^{(\varphi)}$ is the only nonvanishing velocity component and is given by

$$[v^{(\varphi)}]^2 = v_c^2 = -\frac{g_{\varphi\varphi}}{g_{tt}}\omega^2. \quad (9)$$

v_c represents the circular speed (rotation profile) of the particles measured by an inertial observer far from the source, and it is a physical parameter of interest, especially in the description of galaxies, related to the circular motion of test particles along geodesics on the galactic plane.

The angular speed ω^2 can be calculated considering the geodesic motion of the particles. For equatorial orbits, the Lagrangian for a massive test particle is

$$2\mathcal{L} = g_{ab}\dot{x}^a\dot{x}^b = -e^{2\nu}\dot{t}^2 + e^{2\lambda}(\dot{r}^2 + r^2\dot{\varphi}^2), \quad (10)$$

where the overdot denotes derivative with respect to the proper time τ . The Lagrange's equations

$$\frac{d}{d\tau} \left(\frac{\partial \mathcal{L}}{\partial \dot{x}^a} \right) - \frac{\partial \mathcal{L}}{\partial x^a} = 0 \quad (11)$$

yield two constants of motion

$$E = -p_t/m = e^{2\nu}\dot{t}, \quad (12a)$$

$$L = p_\varphi/m = e^{2\lambda}r^2\dot{\varphi}, \quad (12b)$$

where E represents the relativistic specific energy and L the specific angular momentum. Therefore, the Lagrangian can be written as

$$2\mathcal{L} = e^{2\lambda}\dot{r}^2 + e^{-2\lambda}\frac{L^2}{r^2} - e^{-2\nu}E^2. \quad (13)$$

Normalizing u^a , that is requiring $g_{ab}u^au^b = -1$, we obtain

$$e^{2\nu+2\lambda}\dot{r}^2 + e^{2\nu} \left(1 + e^{-2\lambda}\frac{L^2}{r^2} \right) = E^2. \quad (14)$$

This expression allows to define an effective potential V_{eff} as

$$V_{eff} = e^{2\nu} \left(1 + e^{-2\lambda}\frac{L^2}{r^2} \right). \quad (15)$$

For a circular motion have that

$$E^2 = e^{2\nu} \left(1 + e^{-2\lambda}\frac{L^2}{r^2} \right). \quad (16)$$

Assuming the Lagrangian as $\tilde{\mathcal{L}} = 2\mathcal{L} + 1$ and using the condition of normalizing (14), the radial motion equation for circular orbits (extreme motion) reads

$$\frac{dV_{eff}}{dr} = 0. \quad (17)$$

This condition implies

$$\frac{L^2}{r^2} = \frac{r\nu_{,r}e^{2\lambda-2\nu}E^2}{1+r\lambda_{,r}}. \quad (18)$$

From Eqs. (16) and (18) we find

$$E^2 = \frac{e^{2\nu}}{1 - \frac{r\nu_{,r}}{1+r\lambda_{,r}}}, \quad (19a)$$

$$L^2 = \frac{r^3\nu_{,r}e^{2\lambda}}{1+r(\lambda_{,r}-\nu_{,r})}. \quad (19b)$$

By using the conserved quantities (12a) and (12b), and the expression (18) we obtain

$$\omega^2 = \frac{\dot{\varphi}^2}{\dot{t}^2} = e^{4(\nu-\lambda)} \frac{L^2}{r^4 E^2} = -\frac{g_{tt,r}}{g_{\varphi\varphi,r}}. \quad (20)$$

Thus, for motion of particles in circular orbit the tangential velocity is given by

$$v_c^2 = \frac{r\nu_{,r}}{1+r\lambda_{,r}}, \quad (21)$$

and the angular momentum can be cast as

$$L^2 = \frac{r^2 e^{2\lambda} v_c^2}{1-v_c^2}. \quad (22)$$

In addition, in order to have stable circular orbits against radial perturbations the following condition must be satisfied

$$\left. \frac{d^2 V_{eff}}{dr^2} \right|_{extr} > 0, \quad (23)$$

or explicitly

$$\nu_{,rr} + \nu_{,r} \left(2\lambda_{,r} - 2\nu_{,r} + \frac{3}{r} - \frac{\lambda_{,r} + r\lambda_{,rr}}{1+r\lambda_{,r}} \right) > 0. \quad (24)$$

In terms of the angular momentum the stability condition (24) reads

$$\frac{dL^2}{dr} > 0, \quad (25)$$

which is an extension of the Rayleigh criteria of stability of a fluid in rest in a gravitational field [14–16].

For non-circular orbits on the equatorial plane the velocity \mathbf{v} of the particles has two components, the radial velocity $[v^{(r)}]^2 = v_r^2 = -(g_{rr}/g_{tt})(dr/dt)^2$ and the tangential velocity $v^{(\varphi)} = v_c$, then for the geodesic motion of the particles the speed v is given by

$$v^2 = v_r^2 + v_c^2 = \frac{r\nu_{,r}}{1+r\lambda_{,r}} + \frac{(g_{\varphi\varphi}g_{rr,r} - g_{\varphi\varphi,r}g_{rr})}{g_{tt}g_{\varphi\varphi,r}} \left(\frac{dr}{dt} \right)^2 - \frac{2g_{\varphi\varphi}g_{rr}}{g_{tt}g_{\varphi\varphi,r}} \left(\frac{d^2r}{dt^2} \right). \quad (26)$$

III. ANISOTROPIC FLUID SPACETIMES

For a given physical circular speed profile v_c , the metric function ν can be obtained, for circular geodesics, by integrating (21) which, for the metric potential λ (4) and with $\phi = \Phi$, can be cast as

$$\nu_{,r} = \frac{v_c^2 (1 - \frac{\Phi}{2} - v_N^2)}{r (1 - \frac{\Phi}{2})}, \quad (27)$$

where $v_N^2 = r\Phi_{,r}$ is the Newtonian circular speed. Like the energy density, v_c can be chosen by also requiring that in the Newtonian limit it reduces to its Newtonian value v_N . Any tangential velocity profile of the form

$$v_c^2 = \frac{v_N^2 (1 - \frac{\Phi}{2})}{(1 - \frac{\Phi}{2} - v_N^2)} F(\Phi), \quad (28)$$

with $F(0) = 1$ satisfies such condition. It follows that $\nu = \int F(\Phi) d\Phi + C$, where C is a constant of integration which is chosen so that the metric is asymptotically flat. The form of the tangential speed and also the parameters must be chosen so that the matter fields, in order to be physically meaningful, satisfy the energy conditions: $\rho \geq 0$ (weak energy condition), $|\rho| \geq |p_i|$ (dominant energy condition) and $\rho + p_r + p_\theta + p_\varphi \geq 0$ (strong energy condition). Moreover, we must obtain positive values (pressure) for the principal stresses and stable circular orbits. In general, the spacetimes built using this approach represent anisotropic fluid matter configurations. To obtain a perfect fluid source, equality between equations (2b) and (2c) (condition of isotropy pressure) must also be required. Accordingly, only in some special cases spacetimes are obtained that have as source an isotropic fluid.

A particular expression for F for which ν can also be obtained analytically is $F = P_\alpha(\cos \Phi)$ (α -type spacetimes), where P_α are the Legendre polynomials for which $P_\alpha(1) = 1$. Powers of these functions are also possible spacetimes. Integrating (27), we obtain, for instance, for the first four Legendre polynomials

$$\nu_0 = \Phi, \quad (29a)$$

$$\nu_1 = \sin \Phi, \quad (29b)$$

$$\nu_2 = \frac{1}{4} \left(\Phi + \frac{3}{2} \sin 2\Phi \right), \quad (29c)$$

$$\nu_3 = \frac{1}{6} (5 \cos^2 \Phi + 1) \sin \Phi. \quad (29d)$$

For the first member of the family $\alpha = 0$ and weak gravitational fields $\Phi \ll 1$, $e^{2\nu} \approx 1 + 2\Phi$. Therefore, this spacetime has a well-defined Newtonian limit.

Another simple expression for F is $F(\Phi) = (1 - \Phi/2)^{\beta-2}$ (β -type spacetimes), where β is a constant. In this case

$$\nu = \begin{cases} -2 \ln(1 - \frac{\Phi}{2}), & \beta = 1, \\ \frac{2}{\beta-1} [1 - (1 - \frac{\Phi}{2})^{\beta-1}], & \text{otherwise.} \end{cases} \quad (30)$$

The case $\beta = 1$ was studied in Ref. [4] and describes a Majumdar-Papapetrou type spacetime. The second member of the family $\beta = 2$ is the same as the above spacetime $\alpha = 0$.

A third family of spacetimes is when $F(\Phi) = \frac{(1-\Phi/2)^{\gamma-2}}{(1+\Phi/2)^\gamma}$ (γ -type spacetimes). We obtain

$$\nu = \begin{cases} \ln \left[(1 + \frac{\Phi}{2})(1 - \frac{\Phi}{2})^{-1} \right], & \gamma = 1, \\ \frac{1}{\gamma-1} \left[1 - \left(\frac{1-\Phi/2}{1+\Phi/2} \right)^{\gamma-1} \right], & \text{otherwise.} \end{cases} \quad (31)$$

The case $\gamma = 1$ with $\Phi = -MG/\sqrt{a^2 + r^2}$ (the Plummer model [17]), being a a constant with the dimensions of length, corresponds to the Buchdahl's perfect fluid solution [18], a relativistic analog of a classical polytrope of index 5. Anisotropic spacetimes for this member of the family were studied in Refs. [2, 3].

Thus, given a seed Newtonian potential-density pair (Φ, ρ_N) and its corresponding circular speed profile v_N we can construct, for circular geodesics, the relativistic version of different spherically symmetric physical structures. For noncircular geodesics the expression for the speed v of the particles, Eq. (26), differs substantially from (21) and consequently the compute of ν from an imposed speed profile v which in Newtonian limit approach its Newtonian counterpart is more involved.

A. Relativistic thick spherical shell models

We consider the potential-density pair

$$\Phi = -\frac{GM}{b + (a^n + r^n)^{1/n}}, \quad (32a)$$

$$\rho_N = \frac{M}{4\pi} \frac{r^{n-2} [2br^n + (n+1)(b+d)a^n]}{d^{2n-1}(b+d)^3}, \quad (32b)$$

where

$$d = (a^n + r^n)^{1/n}, \quad (33)$$

$n \geq 1$ and a and b are a non-zero constants with the dimensions of length. The models with $n > 2$ describe a shell-like matter distribution. The case $a = b$ corresponds to the generalized isochrone models presented in reference [19] and $b = 0$ are generalized Plummer models [20]. The latter include the Hernquist model ($n = 1$) [21] and the Plummer model ($n = 2$) [17] as particular cases. Such potential-density pairs have been used as successful analytic models for elliptical galaxies and bulges of disk galaxies. The Newtonian circular speed is given by

$$v_N^2 = \frac{MG r^n}{d^{n-1}(b+d)^2}. \quad (34)$$

In the relativistic case, we show below the main physical quantities associated to the systems to the first member $\alpha = 0$ of the first family of spacetimes. Since the expression are huge, other cases will be analyzed graphically. Thus, when $\alpha = 0$ we have

$$\tilde{\rho} = \frac{8\tilde{r}^{n-2}(\tilde{b} + \tilde{d})^2 [2\tilde{b}\tilde{r}^n + (n+1)(\tilde{b} + \tilde{d})\tilde{a}^n]}{\pi\tilde{d}^{2n-1} [2(\tilde{b} + \tilde{d}) + 1]^5}, \quad (35a)$$

$$\tilde{p}_r = \frac{8\tilde{r}^{n-2}(\tilde{b} + \tilde{d}) \left[(\tilde{b} - \frac{1}{2})\tilde{r}^n + (2\tilde{b} + \tilde{d} + \frac{1}{2})\tilde{a}^n + \tilde{b}(\tilde{b} + \frac{1}{2})\tilde{d}^{n-1} \right]}{\pi\tilde{d}^{2(n-1)} [2(\tilde{b} + \tilde{d}) + 1]^6}, \quad (35b)$$

$$\begin{aligned} \tilde{p}_\varphi = & \frac{4\tilde{r}^{n-2}}{\pi\tilde{d}^{2n-1} [2(\tilde{b} + \tilde{d}) + 1]^6} \left[n\tilde{a}^n\tilde{d}^3 + \left((\tilde{b} + \frac{3}{2})\tilde{r}^n + 3n(\tilde{b} + \frac{1}{6})\tilde{a}^n \right) \tilde{d}^2 \right. \\ & \left. + \left(2(\tilde{b} + \frac{1}{2})^2\tilde{r}^n + 3n\tilde{b}(\tilde{b} + \frac{1}{3})\tilde{a}^n \right) \tilde{d} + \tilde{b}^2(\tilde{b} + \frac{1}{2}) (\tilde{r}^n + n\tilde{a}^n) \right], \end{aligned} \quad (35c)$$

$$v_c^2 = \frac{\tilde{r}^n [2(\tilde{b} + \tilde{d}) + 1]}{(\tilde{b} + \tilde{d}) \left[(2(\tilde{b} + \tilde{d}) + 1) \tilde{d}^{n-1}(\tilde{b} + \tilde{d}) - 2\tilde{r}^n \right]}, \quad (35d)$$

$$\tilde{L}^2 = \frac{\tilde{r}^{n+2} [2(\tilde{b} + \tilde{d}) + 1]^5}{16(\tilde{b} + \tilde{d})^4 \left[(2(\tilde{b} + \tilde{d}) + 1) \tilde{d}^{n-1}(\tilde{b} + \tilde{d})^2 - (4(\tilde{b} + \tilde{d}) + 1) \tilde{r}^n \right]}, \quad (35e)$$

where $\tilde{\rho} = G^3 M^2 \rho$, $\tilde{p}_r = G^3 M^2 p_r$, $\tilde{p}_\varphi = G^3 M^2 p_\varphi$, $\tilde{L} = L/(GM)$, $\tilde{r} = r/(GM)$, $\tilde{a} = a/(GM)$, $\tilde{b} = b/(GM)$ and $\tilde{d} = d/(GM)$. We see that the energy density always is a positive quantity in according to the weak energy condition and in order to have pressures everywhere we must take $\tilde{b} \geq 1/2$.

In figures 1, 3 and 5 we show, as functions of \tilde{r} , the curves of the relativistic energy density $\tilde{\rho}$, the radial pressure \tilde{p}_r and the tangential pressure \tilde{p}_φ for the relativistic thick shells with $\alpha = 0, 1$, and $\beta = 3$ and parameters $\tilde{a} = \tilde{b} = 0.6, 0.8, 1.2, \tilde{a} = \tilde{b} = 2, 3, 4$, and $\tilde{a} = \tilde{b} = 0.7, 0.9, 1.2$, respectively, with $n = 3$ and $n = 6$. Such quantities vanish at the origin which suggests a shell-like matter distribution, then increase rapidly, reach a maximum and later decrease rapidly with the radius which permits to define a cut off radius r_c and, in principle, to consider these structures as compact objects. As the value of the parameters \tilde{a} and \tilde{b} are increased, the shells are smoothed out and become more concentrated when the parameter n is increased. We also observe that for the first family of spacetimes it is always possible to find in all the cases parameters for which the principal stresses are positive quantities everywhere, but for the other two families, except for $\beta = 2$ and $\gamma = 1$, it was found that far from the central region the tangential

stresses take very small negative values. In this case, the cut off radius of the structures could be defined just before the azimuthal stresses become negative.

In figures 2, 4 and 6 we plot the rotation curves v_c^2 and the specific angular momentum \tilde{L}^2 for the same value of parameters. As the value of the parameters \tilde{a} and \tilde{b} are increased, the circular speed decreases and increases with the increase of the parameter n . For this value of parameters also the circular speed of particles is a quantity less than the speed of light in according to the dominant energy condition and the orbits of the particles are stable. However, the orbits can become unstable as the value of the parameters \tilde{a} and \tilde{b} decrease.

IV. A RELATIVISTIC MODEL OF GALAXY

In cylindrical coordinates (t, φ, R, z) the metric (1) takes the form

$$ds^2 = -e^{2\nu} dt^2 + e^{2\lambda} (R^2 d\varphi^2 + dR^2 + dz^2), \quad (36)$$

where ϕ is function of R and z only. The Einstein's gravitational field equations yield the following non-zero components of the energy-momentum tensor

$$T^t_t = \frac{1}{4\pi G} e^{-2\lambda} \left[\nabla^2 \lambda + \frac{1}{2} \nabla \lambda \cdot \nabla \lambda \right], \quad (37a)$$

$$T^\varphi_\varphi = \frac{1}{8\pi G} e^{-2\lambda} \left[\nabla \nu \cdot \nabla \nu + \nabla^2 \nu + \nabla^2 \lambda - \frac{1}{R} (\lambda_{,R} + \nu_{,R}) \right], \quad (37b)$$

$$T^R_R = \frac{1}{8\pi G} e^{-2\lambda} \left[\lambda_{,zz} + \nu_{,zz} + \lambda_{,R}^2 + \nu_{,z}^2 + 2\lambda_{,R}\nu_{,R} + \frac{1}{R} (\lambda_{,R} + \nu_{,R}) \right], \quad (37c)$$

$$T^z_z = \frac{1}{8\pi G} e^{-2\lambda} \left[\lambda_{,RR} + \nu_{,RR} + \lambda_{,z}^2 + \nu_{,R}^2 + 2\lambda_{,z}\nu_{,z} + \frac{1}{R} (\lambda_{,R} + \nu_{,R}) \right], \quad (37d)$$

$$T^R_z = -\frac{1}{8\pi G} e^{-2\lambda} [\lambda_{,Rz} + \nu_{,Rz} - (\lambda_{,z} + \nu_{,z}) \lambda_{,R} + \nu_{,R}\nu_{,z} - \lambda_{,z}\nu_{,R}]. \quad (37e)$$

Now, in order to analyze the matter distributions is necessary to compute the eigenvalues and eigenvectors of the energy-momentum tensor. The eigenvalue problem for the energy-momentum tensor (37a) - (37e) has the solutions

$$\lambda_t = T^t_t, \quad (38a)$$

$$\lambda_\varphi = T^\varphi_\varphi, \quad (38b)$$

$$\lambda_{R,z} = \frac{T \pm \sqrt{D}}{2}, \quad (38c)$$

where

$$T = T^R_R + T^z_z, \quad (39a)$$

$$D = (T^R_R - T^z_z)^2 + 4(T^R_z)^2. \quad (39b)$$

The corresponding eigenvectors are

$$\mathbf{V}_{ax} = \frac{1}{\sqrt{-g_{tt}}} (1, 0, 0, 0), \quad (40a)$$

$$\mathbf{X}_{ax} = \frac{1}{\sqrt{g_{\varphi\varphi}}} (0, 1, 0, 0), \quad (40b)$$

$$\mathbf{Y}_{ax} = \frac{1}{\sqrt{g_{RR}(1 + n_+^2)}} (0, 0, 1, n_+), \quad (40c)$$

$$\mathbf{Z}_{ax} = \frac{1}{\sqrt{g_{RR}(1 + n_-^2)}} (0, 0, 1, n_-), \quad (40d)$$

where

$$n_{\pm} = \frac{T^z_z - T^R_R \pm \sqrt{D}}{2T^R_z}. \quad (41)$$

In terms of the above proper observer, the energy density is given by $\rho = -\lambda_t$ and the principal stresses by $p_i = \lambda_i$. For the particular form of λ (4) the energy density is given by the nonlinear Poisson type equation (5) and again taking the energy density profile as (6), then it follows $(\phi, \rho_0) = (\Phi, \rho_N)$. Similarly, for equatorial, circular orbit the circular speed and the specific angular momentum are given by

$$v_c^2 = \frac{R\nu_{,R}}{1 + R\lambda_{,R}}, \quad (42a)$$

$$L^2 = \frac{R^2 e^{2\lambda} v_c^2}{1 - v_c^2}, \quad (42b)$$

and the stability condition reads

$$\frac{dL^2}{dR} > 0. \quad (43)$$

Following the approach presented in the above section, the metric potential ν can also be take in the particular form (31) in cylindrical coordinates.

As an example, we consider the Newtonian Galactic potential composite by the sum of three components

$$\Phi = \Phi_B + \Phi_D + \Phi_H, \quad (44)$$

where Φ_B corresponds to the central spherical bulge potential, Φ_D describes the thick disk and Φ_H the spherical dark halo. The bulge and disk potentials are given by Plummer and Miyamoto-Nagai models [8, 9, 17]

$$\Phi_B = -\frac{GM_B}{\sqrt{r^2 + b_B^2}}, \quad (45a)$$

$$\Phi_D = -\frac{GM_D}{\sqrt{R^2 + \left(a_D + \sqrt{z^2 + b_D^2}\right)^2}}, \quad (45b)$$

where $r = \sqrt{R^2 + z^2}$, M_B and M_D are the masses of the components while b_B , a_D , and b_D are non-zero constants with dimensions of length. In addition, a_D and b_D represent length and height scales of the disk-like distribution. The dark matter halo is represented by NFW model which can be cast as

$$\Phi_H = -\frac{GM_H}{r} \ln \left(1 + \frac{r}{a_H} \right), \quad (46)$$

where M_H is the dark halo mass and a_H a scale radius.

In the relativistic case, for simplicity let us consider again the metric potential ν (31) in cylindrical coordinates for the first family of spacetimes when $\alpha = 0$ and $\alpha = 1$. Since the expressions for the main physical quantities are huge, its analysis is better done graphically. However, note that the energy density always is a positive quantity in according to the weak energy condition. The parameter values are choose using as reference the Newtonian potential parameters computed in [22] $a_D = 4.4$, $a_H = 7.7$, $b_B = 0.2672$, $b_D = 0.3084$, $M_b = 443$, $M_d = 2798$ and $M_h = 12474$. Thus, in figures 7, 8, 10 and 11 we graph, as function of $\tilde{R} = R/GM_D$ and $\tilde{z} = z/GM_D$, the surfaces and level curves of the energy density $\tilde{\rho} = G^3 M_D^2 \rho$ and pressures $\tilde{p}_\varphi = G^3 M_D^2 p_\varphi$, $\tilde{p}_R = G^3 M_D^2 p_R$ and $\tilde{p}_z = G^3 M_D^2 p_z$ for a relativistic galaxy model composite by three components bulge, thick disk and dark matter halo with $\alpha = 0$ and parameters $\tilde{a}_D = a_D/GM_D = 4.4$, $\tilde{a}_H = a_H/GM_D = 7.7$, $\tilde{b}_B = b_B/GM_D = 0.2672$, $\tilde{b}_D = b_D/GM_D = 0.3084$, $\tilde{M}_B = M_B/M_D = 0.1583$ and $\tilde{M}_H = M_H/M_D = 4.4582$, and $\alpha = 1$ with parameters $\tilde{a}_D = 10$, $\tilde{a}_H = 15$, $\tilde{b}_B = 0.5$, $\tilde{b}_D = 0.3048$ and the same values of \tilde{M}_B and \tilde{M}_H . We observer that the energy density, as in the Newtonian case, presents a central cusp and then it decreases rapidly with the radius. The principal stresses are positive quantities which means that we have pressure everywhere, but like the shell models, for the other two families of solutions we find that far from the central region of the structures the tangential stresses can take very small negative values.

In figures 9 and 12 we plot, as function of \tilde{R} , the relativistic circular speed profile v_c , the Newtonian rotation curves v_N , the specific angular momentum $\tilde{L}^2 = L^2/G^2 M_D^2$ and the Newtonian angular momentum $\tilde{L}_N^2 = L_N^2/G^2 M_D^2$, for

the same value of parameters. We observe that when $\alpha = 0$ the relativistic effects increase the circular speed of the particles everywhere whereas that when $\alpha = 1$ such effects initially decrease the tangential speed but after a certain value of \tilde{R} they increase it. Now for stars around a typical galaxy the tangential velocity is about 200 - 300 km/s and accordingly, the geometric effects are expected to be small. For example, in the case of our Galaxy for a radius of $R = 0.4$ kpc which corresponds to a tangential velocity about 260.8 km/s we obtain that the relativistic corrections are in both cases of the order of 9.86×10^{-5} km/s. We believe that for a sufficiently large distance traveled by a star such effects could become significant especially in the central region where the gravitational fields are strong. The graphs also show that the rotation curves are flattened after a certain value of the radial distance as observational data indicate. We also observe that equatorial, circular orbits of test particles moving around the structures are stable against radial perturbations. In addition, since $dL^2/dr > dL_N^2/dr$ everywhere, we see the relativistic circular orbits are more stable than Newtonian ones. It should be noted that we focus our stability study only on radial perturbations because we are considering only circular orbits on the galactic plane $z = 0$ and not the complete structure. A more realistic stability analysis of the matter distribution should be based on perturbations of the energy momentum tensor of the fluid [23] which may be not a trivial task and will be left as a future research subject.

On the other hand, when $\alpha = 0$ we find that as the mass of the dark matter halo or the central bulge mass are increased, keeping the other parameters constant, the models become more relativistic and after certain value of such parameters the dominant energy condition is not satisfied and consequently, the orbits are no longer stable. The opposite occurs when these parameters are decreased. In both scenarios, stresses are always positive quantities (pressure).

Meanwhile, when $\alpha = 1$ we find that as the mass of the dark matter halo is increased the circular speed of the orbits initially decreases but after a certain value of \tilde{R} the models become more relativistic. On the contrary, when such parameter is decreased the models initially become more relativistic but then the tangential speed decreases. In turn, as the central bulge mass is increased one finds that the circular speed also increases in all regions of the structures and conversely as it is decreased the rotation curves also decrease everywhere. In both situations, as those parameters are increased the stresses fast become negative (tension) in the central region of the structures. For example, the models with $m_h = 5.2$ or $m_b = 0.18$ have a central region with tension but for $m_h \leq 5.1$ or $m_b \leq 0.17$ we still have pressure. In turn, as such parameters are decreased, we always have pressure.

V. CONCLUSIONS

Anisotropic fluid sources for conformastat spherically symmetric spacetimes from Newtonian potential-density pairs and its corresponding tangential speed profile were constructed. As simple applications of the method, three analytical families of spherically symmetric spacetimes representing anisotropic matter configurations were presented and applied to the construction of new models of relativistic spherical shells of finite thickness, and of two relativistic galaxy models composite by a central spherical bulge, the thick disk and the dark matter halo, expressing in this case the metric in cylindrical coordinates. The bulge and disk seed potentials were the Plummer and Miyamoto-Nagai models and in the case of the dark matter halo, the NFW model.

In all models considered, the energy conditions are satisfied and were found stable circular orbits. However, we observed that for the first family of spacetimes it is always possible to find in all the cases parameters for which the principal stresses are positive quantities (pressure) everywhere, but for the other two families, except for the cases $\beta = 2$ and $\gamma = 1$, it was found that far from the central region of the structures the azimuthal stresses take very small negative values.

REFERENCES

-
- [1] J. Bičák and B. G. Schmidt, *ApJ* **521**, 708 (1999).
 - [2] D. Vogt and P. S. Letelier, *Mon. Not. Roy. Astron. Soc.* **402**, 1313 (2010).
 - [3] D. Vogt and P. S. Letelier, *Mon. Not. Roy. Astron. Soc.* **406**, 2689 (2010).
 - [4] G. García-Reyes, *Gen. Relativ. Gravit.* **49**, 3, 1-13 (2017).
 - [5] G. García-Reyes, *Eur. Phys. J. Plus* **135**, 931 (2020).
 - [6] D. Vogt and P. S. Letelier, *Mon. Not. Roy. Astron. Soc.* **363**, 268 (2005).
 - [7] G. García-Reyes and Kevin A. Hernández-Gómez, *Int. J. Mod. Phys. D*, Vol. 27, Issue 07, 1850068-1 (2018).
 - [8] M. Miyamoto and R. Nagai, *PASJ* **27**, 533 (1975).

- [9] R. Nagai and M. Miyamoto, PASJ **28**, 1 (1976).
- [10] J. F. Navarro, C. S. Frenk and S. D. M. White, Ap. J. **462**, 563 (1996).
- [11] J. L. Synge, Relativity: The General Theory (North- Holland, Amsterdam, 1960, p. 341).
- [12] H. Stephani, D. Kramer, M. McCallum, C. Hoenselaers, and E. Herlt, Exact Solutions of Einsteins's Field Equations (Cambridge University Press, Cambridge, England, 2003, p. 287).
- [13] J. Binney J and S. Tremaine S, Galactic Dynamics, 2nd edn. Princeton Univ. Press, Princeton, 2008.
- [14] Lord Rayleigh, 1917, Proc. R. Soc. London A, 93, 148.
- [15] L. D. Landau and E. M. Lifshitz, *Fluid Mechanics*(Addison-Wesley, Reading, MA, 1989).
- [16] P. S. Letelier, Phys. Rev. D **68**, 104002 (2003).
- [17] H. C. Plummer, MNRAS **71**, 460 (1911).
- [18] H. A. Buchdahl, ApJ **140**, 1512 (1964).
- [19] J. H. An and N. W. Evans, AJ **131**, 782 (2006).
- [20] Ü. -I. K. Veltmann, Astron. Zh. **56**, 976 (1979).
- [21] L. Hernquist, Ap. J. **356**, 359 (1990).
- [22] A. T. Bajkova and V. V. Bobylev, Astronomy Letters **42**, No. 9, 567 (2016).
- [23] M. Ujevic and P. S. Letelier, Mon. Not. Roy. Astron. Soc. **381**, Issue 4, 1499 (2007).

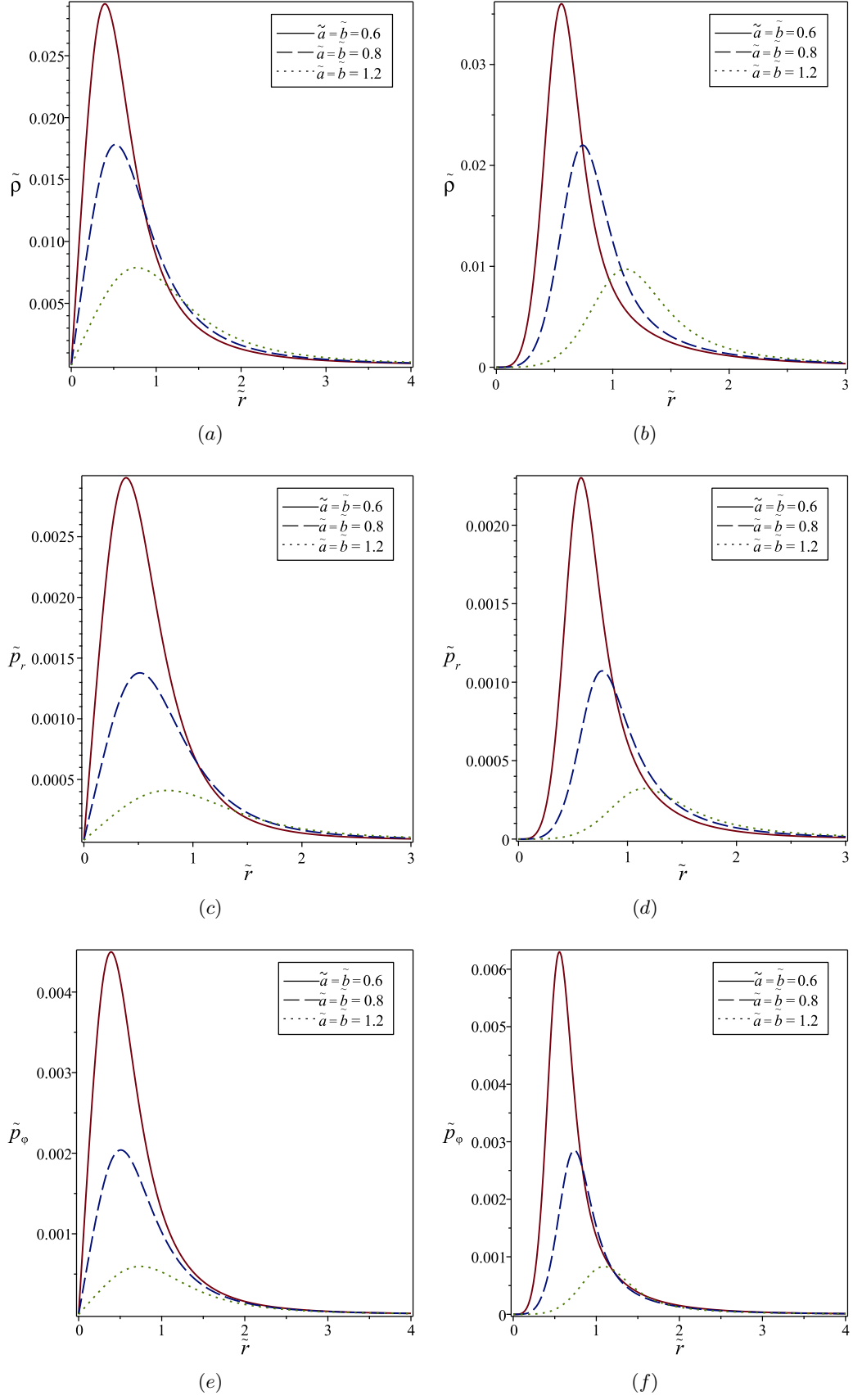


FIG. 1. (a), (b) The relativistic energy density $\tilde{\rho}$, (c), (d) the radial pressure \tilde{p}_r , and (e), (f) the tangential pressure \tilde{p}_φ for the α -type relativistic thick shells with $n = 3$ (left curves) and $n = 6$ (right curves) and parameters $\alpha = 0$, $\tilde{a} = \tilde{b} = 0.6$ (solid curves), 0.8 (dashed curves), and 1.2 (dot curves), as functions of \tilde{r} .

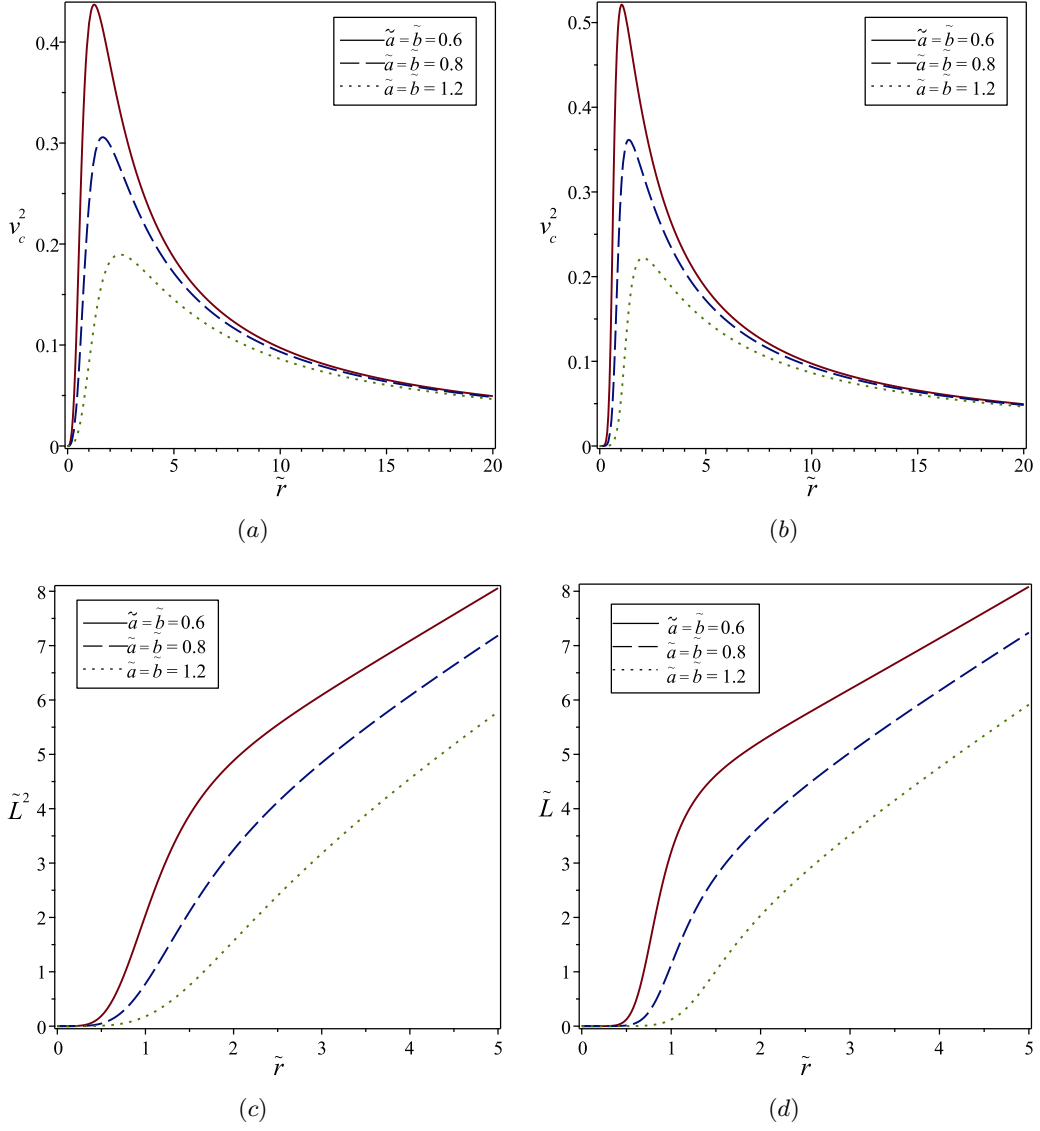


FIG. 2. (a), (b) The rotation curves v_c^2 and (c), (d) the specific angular momentum \tilde{L}^2 for the α -type relativistic thick shells with $n = 3$ (left curves) and $n = 6$ (right curves) and parameters $\alpha = 0$, $\tilde{a} = \tilde{b} = 0.6$ (solid curves), 0.8 (dashed curves), and 1.2 (dot curves), as functions of \tilde{r} .

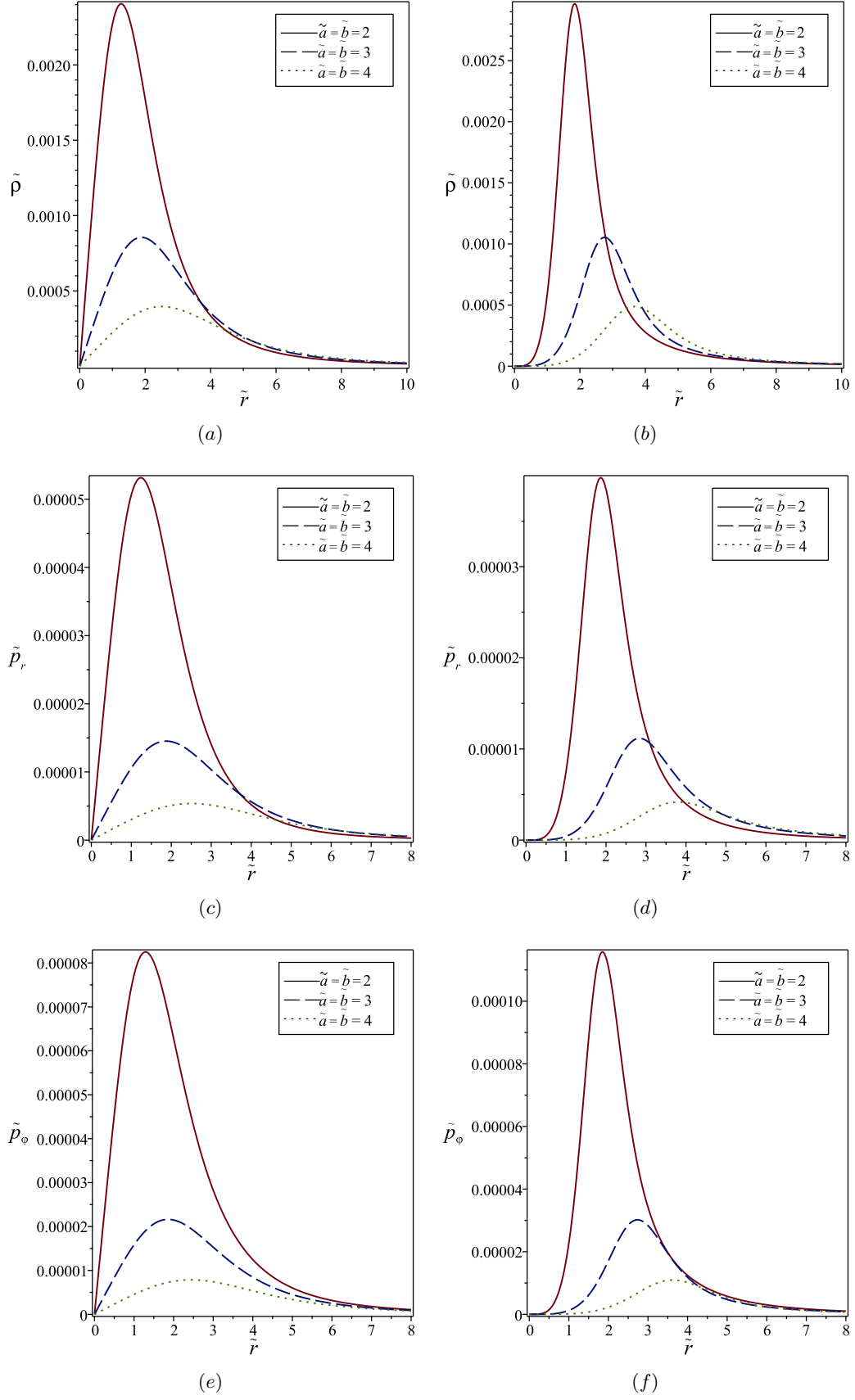


FIG. 3. (a), (b) The relativistic energy density $\tilde{\rho}$, (c), (d) the radial pressure \tilde{p}_r , and (e), (f) the tangential pressure \tilde{p}_φ for the α -type relativistic thick shells with $n = 3$ (left curves) and $n = 6$ (right curves) and parameters $\alpha = 1$, $\tilde{a} = \tilde{b} = 2$ (solid curves), 3 (dashed curves), and 4 (dot curves), as functions of \tilde{r} .

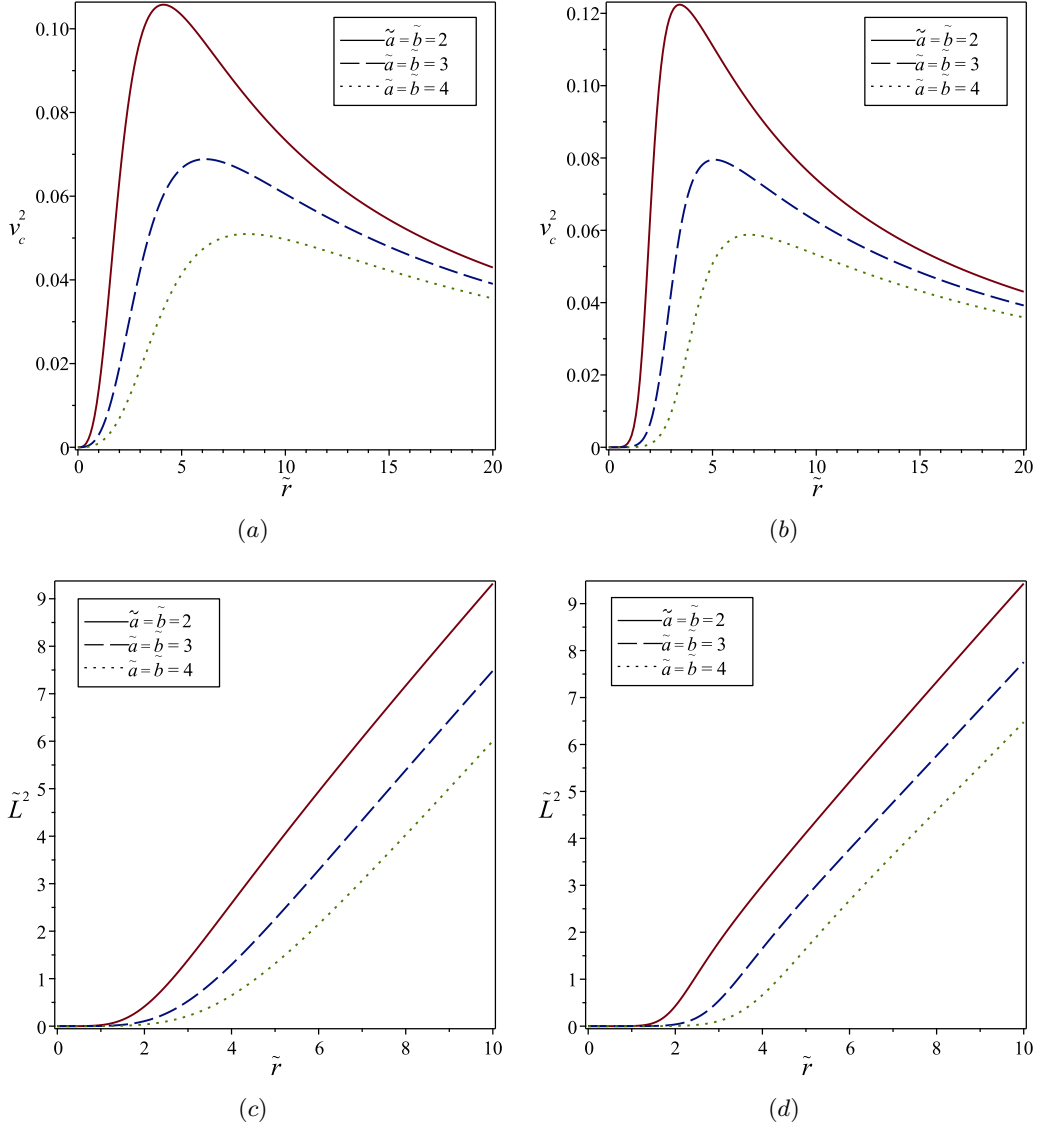


FIG. 4. (a), (b) The rotation curves v_c^2 and (c), (d) the specific angular momentum \tilde{L}^2 for the α -type relativistic thick shells with $n = 3$ (left curves) and $n = 6$ (right curves) and parameters $\alpha = 1$, $\tilde{a} = \tilde{b} = 2$ (solid curves), 3 (dashed curves), and 4 (dot curves), as functions of \tilde{r} .

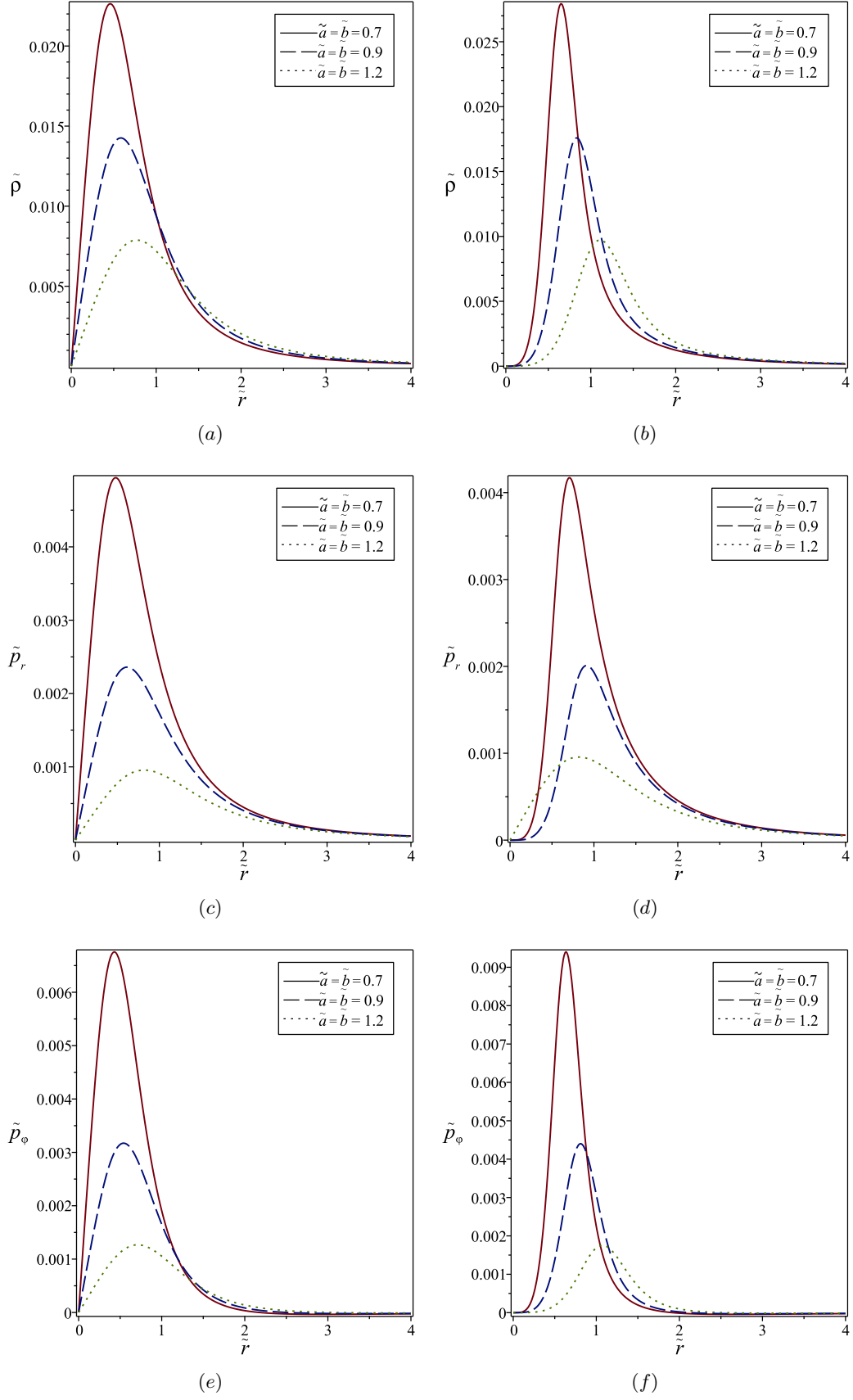


FIG. 5. (a), (b) The relativistic energy density $\tilde{\rho}$, (c), (d) the radial pressure \tilde{p}_r , and (e), (f) the tangential pressure \tilde{p}_φ for the β -type relativistic thick shells with $n = 3$ (left curves) and $n = 6$ (right curves) and parameters $\beta = 3$, $\tilde{a} = \tilde{b} = 0.7$ (solid curves), 0.9 (dashed curves), and 1.2 (dot curves), as functions of \tilde{r} .

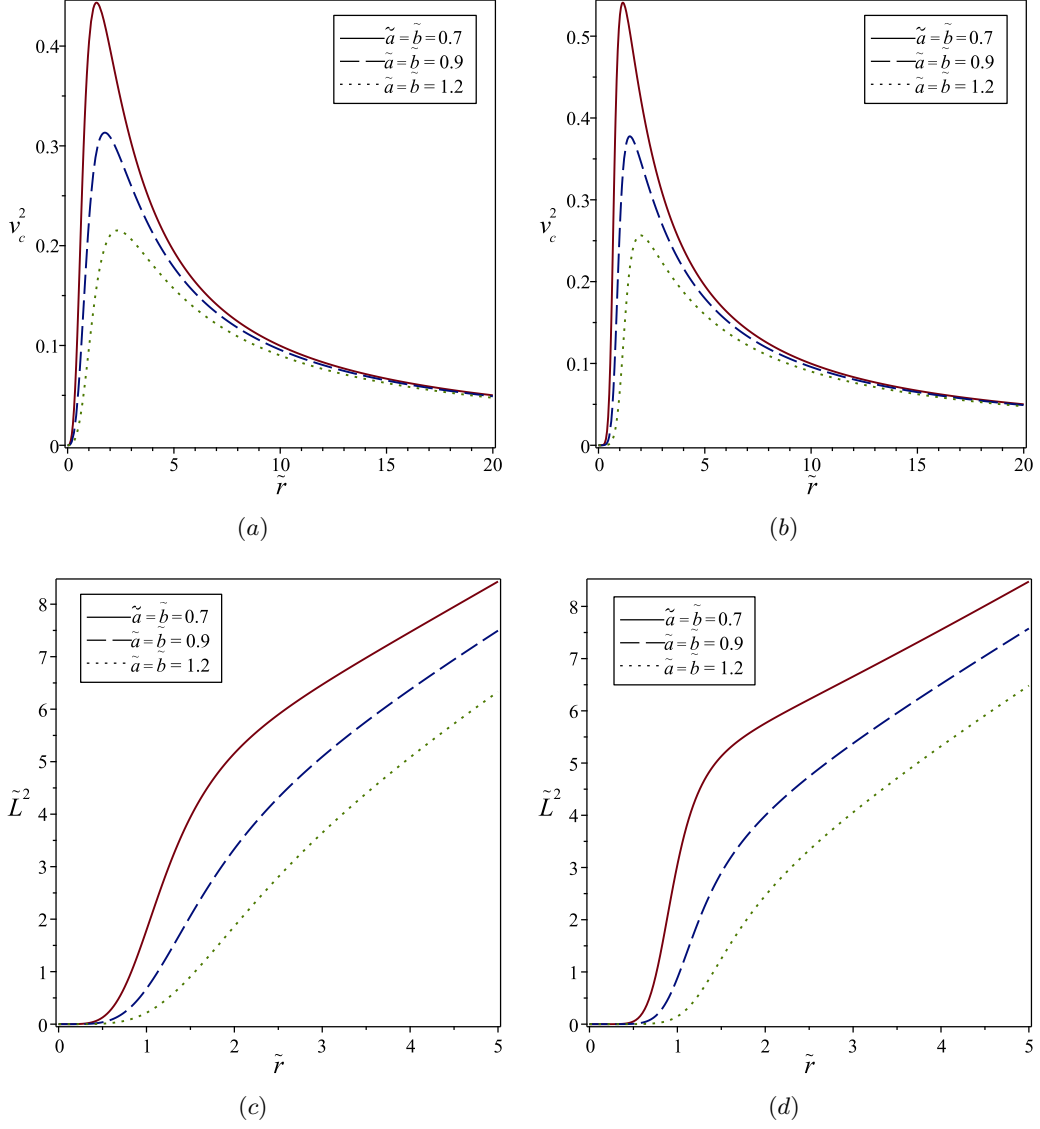


FIG. 6. (a), (b) The rotation curves v_c^2 and (c), (d) the specific angular momentum \tilde{L}^2 for the β -type relativistic thick shells with $n = 3$ (left curves) and $n = 6$ (right curves) and parameters $\beta = 3$, $\tilde{a} = \tilde{b} = 0.7$ (solid curves), 0.9 (dashed curves), and 1.2 (dot curves), as functions of \tilde{r} .

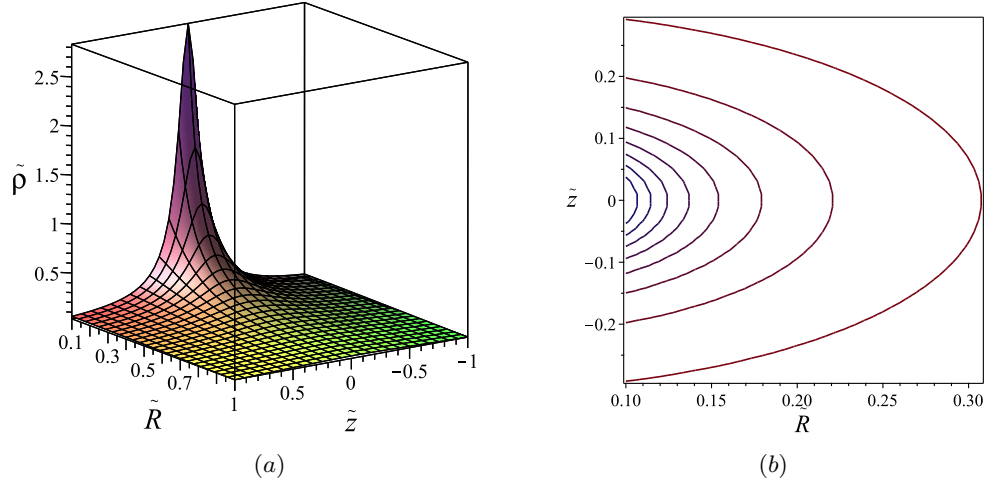


FIG. 7. (a) The relativistic energy density profile $\tilde{\rho}$ and (b) the isodensity curves for a $\alpha = 0$ type relativistic galaxy model composite by three components bulge, thick disk and dark matter halo, as functions of \tilde{R} and \tilde{z} .

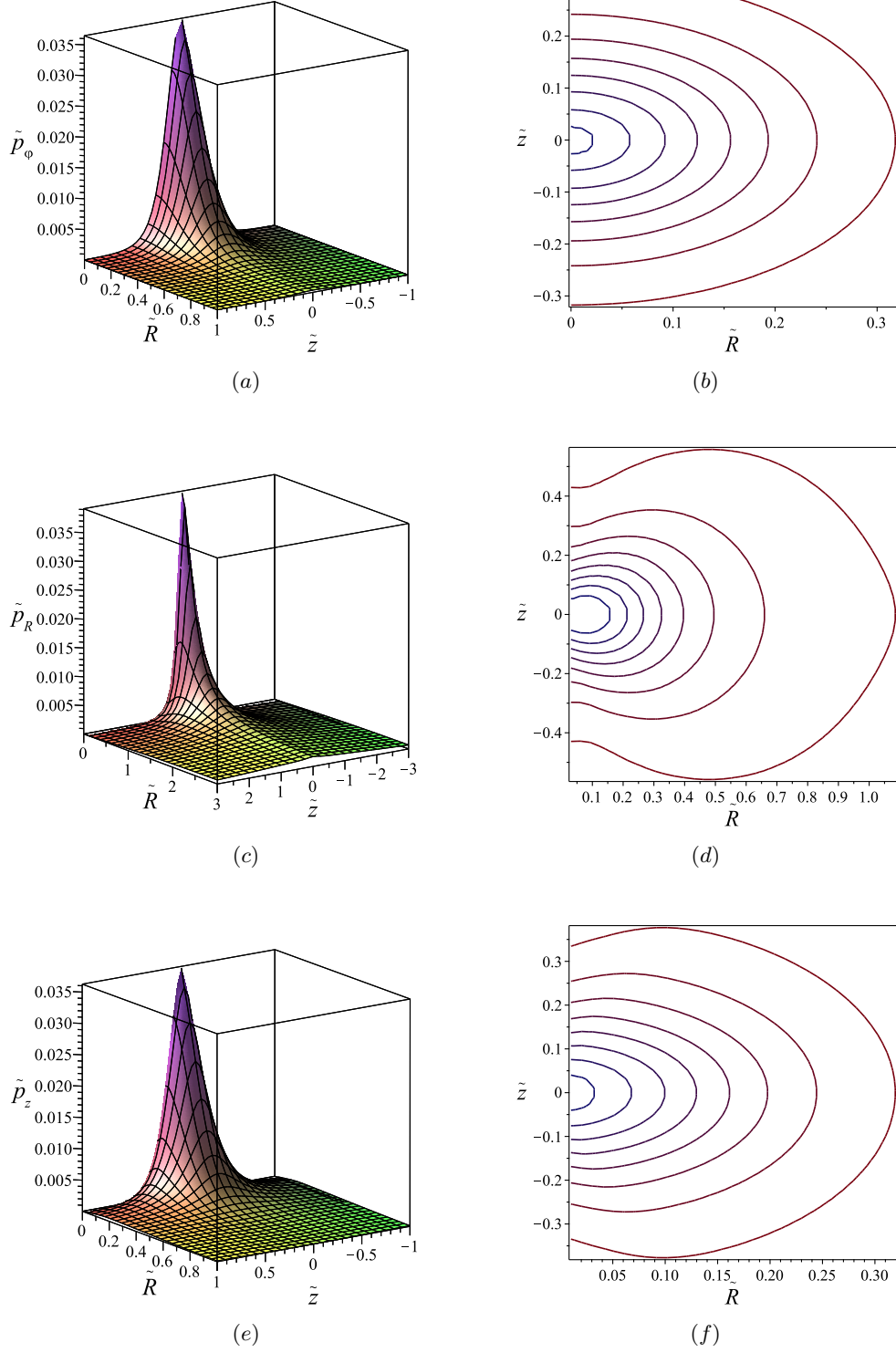


FIG. 8. The surfaces and level curves of the pressures \tilde{p}_ϕ , \tilde{p}_R and \tilde{p}_z , as functions of \tilde{R} and \tilde{z} , for a $\alpha = 0$ type relativistic galaxy model composite by three components bulge, thick disk and dark matter halo.

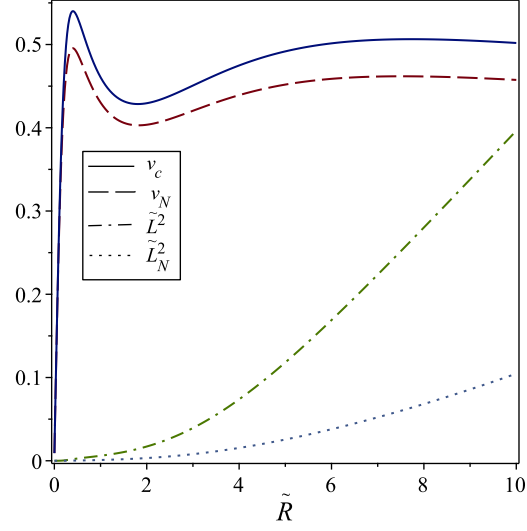


FIG. 9. The relativistic circular speed v_c (solid curve), the Newtonian rotation curve v_N (dashed curve), the relativistic and Newtonian specific angular momenta \tilde{L}^2 (dashed-dotted curve) and \tilde{L}_N^2 (dotted curve), scaled by 200, for the system composite by bulge, thick disk and dark matter halo, with $\alpha = 0$, as functions of \tilde{R} .

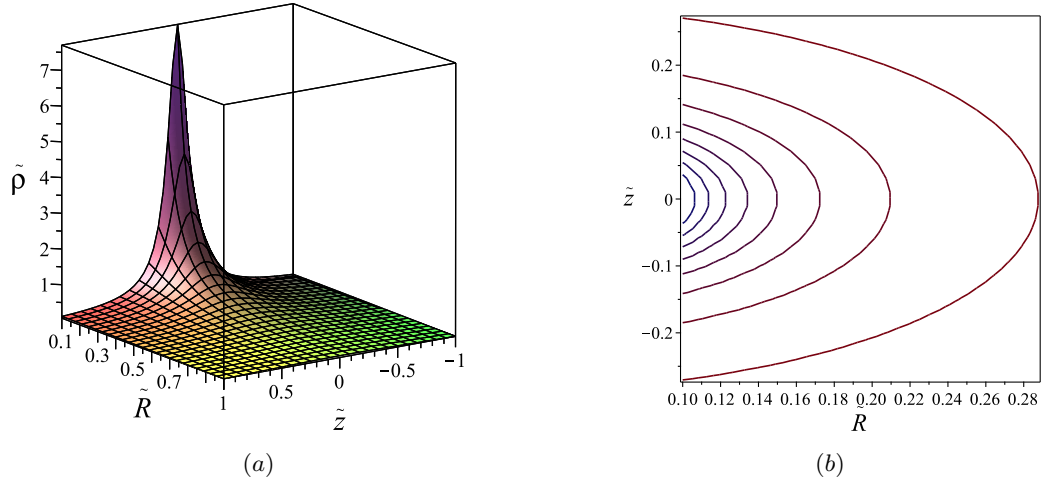


FIG. 10. (a) The relativistic energy density profile $\tilde{\rho}$ and (b) the isodensity curves for a $\alpha = 1$ type relativistic galaxy model composite by three components bulge, thick disk and dark matter halo, as functions of \tilde{R} and \tilde{z} .

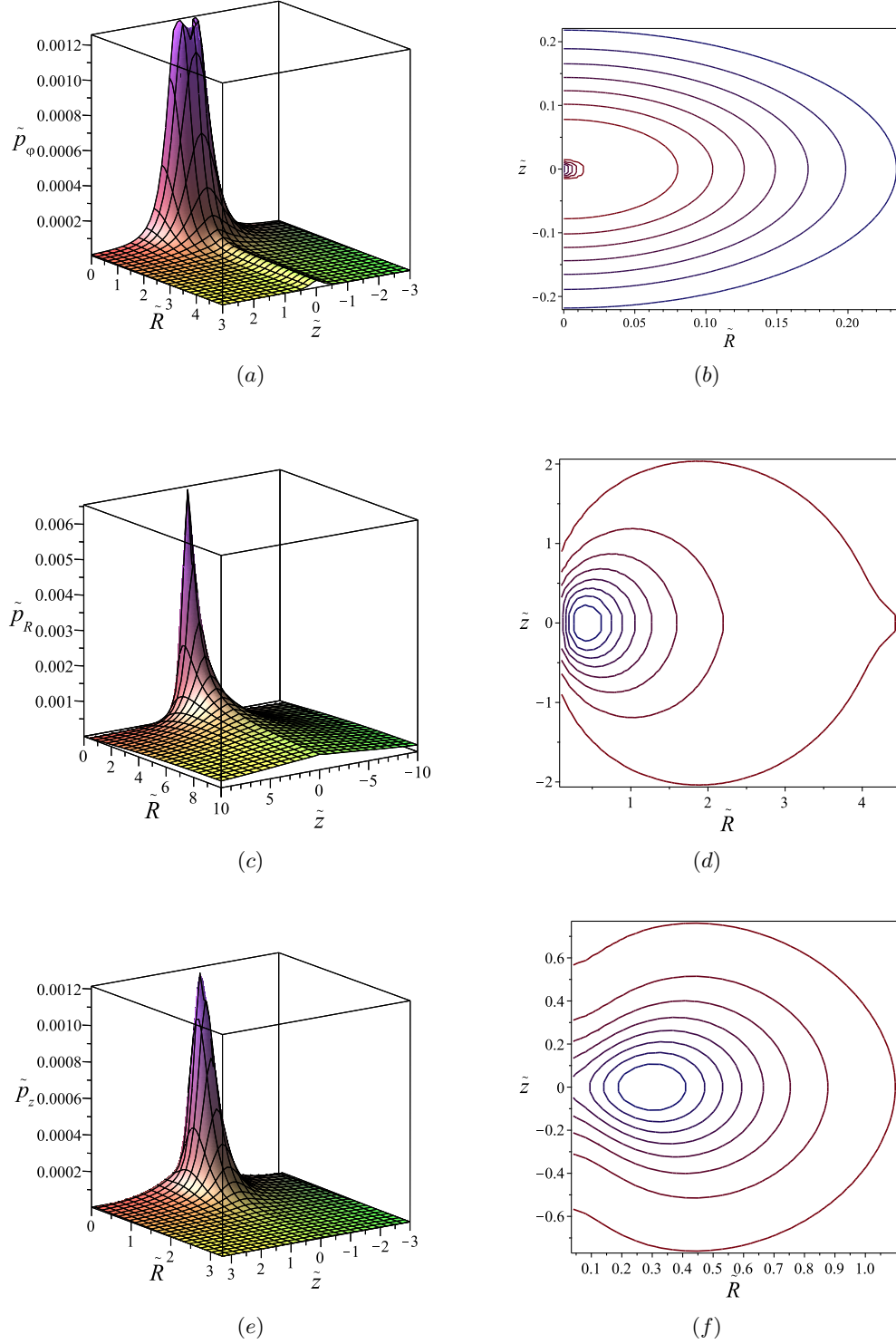


FIG. 11. The surfaces and level curves of the pressures \tilde{p}_ϕ , \tilde{p}_R and \tilde{p}_z , as functions of \tilde{R} and \tilde{z} , for a $\alpha = 1$ type relativistic galaxy model composite by three components bulge, thick disk and dark matter halo.

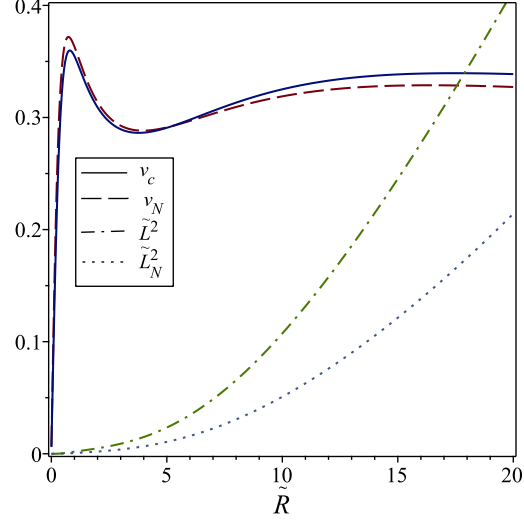


FIG. 12. The relativistic circular speed v_c (solid curve), the Newtonian rotation curve v_N (dashed curve), the relativistic and Newtonian specific angular momenta \tilde{L}^2 (dashed-dotted curve) and \tilde{L}_N^2 (dotted curve), scaled by 200, for the system composite by bulge, thick disk and dark matter halo, with $\alpha = 1$, as functions of \tilde{R} .